ELSEVIER

www.elsevier.nl/locate/carres

Carbohydrate Research 324 (2000) 53–65

CARBOHYDRATE RESEARCH

NMR spectroscopy, molecular dynamics, and conformation of a synthetic octasaccharide fragment of the O-specific polysaccharide of *Shigella dysenteriae* type 1

Bruce Coxon [a,*], Nese Sari [a], Gyula Batta [b], Vince Pozsgay [c]

[a] *Biotechnology Division, National Institute of Standards and Technology, 100 Bureau Drive Stop 8311, Gaithersburg, MD 20899-8311, USA*

[b] *Research Group for Antibiotics of the Hungarian Academy of Sciences, Debrecen, Hungary*

[c] *Laboratory of Developmental and Molecular Immunity, National Institute of Child Health and Human Development, National Institutes of Health, Bethesda, MD 20892-2720, USA*

Received 12 August 1999; accepted 30 September 1999

Abstract

A synthetic octasaccharide fragment (**2**) of the O-specific polysaccharide (**1**) of *Shigella dysenteriae* type 1 has been studied as its methyl glycoside by one- and two-dimensional homo- and heteronuclear NMR spectroscopy. Complete ^{1}H and ^{13}C NMR assignments have been generated, and the ^{13}C spin–lattice relaxation times have been measured for the octasaccharide **2**. A congener (**6**) of this octasaccharide containing one D-galactose residue with a specific ^{13}C label at C-1 has been synthesized and used to measure interglycosidic $^{13}C-^{1}H$ coupling by the 2D *J*-resolved ^{1}H NMR method. From the NMR data, three types of conformational restraints were developed: (a) 29 inter-residue, distance restraints; (b) 48 intra-residue, ring atom dihedral angle restraints, and (c) one heteronuclear, inter-residue dihedral angle restraint. The use of these restraints in a restrained molecular dynamics computation with simulated annealing yielded a conformation resembling a short, irregular spiral, with methyl substituents on the exterior. Published by Elsevier Science Ltd.

Keywords: ^{13}C-Labeling; Conformation; NMR spectroscopy; Octasaccharide; Restrained molecular dynamics; *Shigella dysenteriae* type 1; Simulated annealing; TOCSY; T-ROESY

1. Introduction

In a program aimed at developing a synthetic saccharide–protein conjugate vaccine [1] against the enteric pathogen, *Shigella dysenteriae* type 1, which can cause endemic and epidemic diarrhea and dysentery, we have reported the synthesis of a number of oligosaccharide fragments of the O-specific polysaccharide **1** of this pathogen [2–10]. Human serum albumin conjugates of the octa-, dodeca- and hexadeca-saccharide fragments have shown significant ability to induce IgG antibodies in mice against the lipopolysaccharide of *S. dysenteriae* type 1 [1].

* Corresponding author. Tel.: +1-301-975-3135; fax: +1-301-330-3447.

E-mail address: bruce.coxon@nist.gov (B. Coxon)

0008-6215/00/$ - see front matter Published by Elsevier Science Ltd.
PII: S0008-6215(99)00278-5

3)-α-L-Rha*p*-(1→2)-α-D-Gal*p*-(1→3)-α-D-GlcN*p*-(1→2)-α-L-Rha*p*-(1→ (**1**)

An important observation was that the protein conjugates of the synthetic saccharides elicit higher levels of IgG lipopolysaccharide antibodies than those of the O-specific polysaccharide from *S. dysenteriae* type 1 [1]. NMR studies of the structures and conformations of these saccharides are of interest in connection with efforts to define the molecular specificities of antigen–antibody binding [11,12].

This paper presents NMR and molecular modeling results for the octasaccharide **2** that contains two consecutive repeating units of the O-specific polysaccharide (see Scheme 1). Using similar methods, we have previously

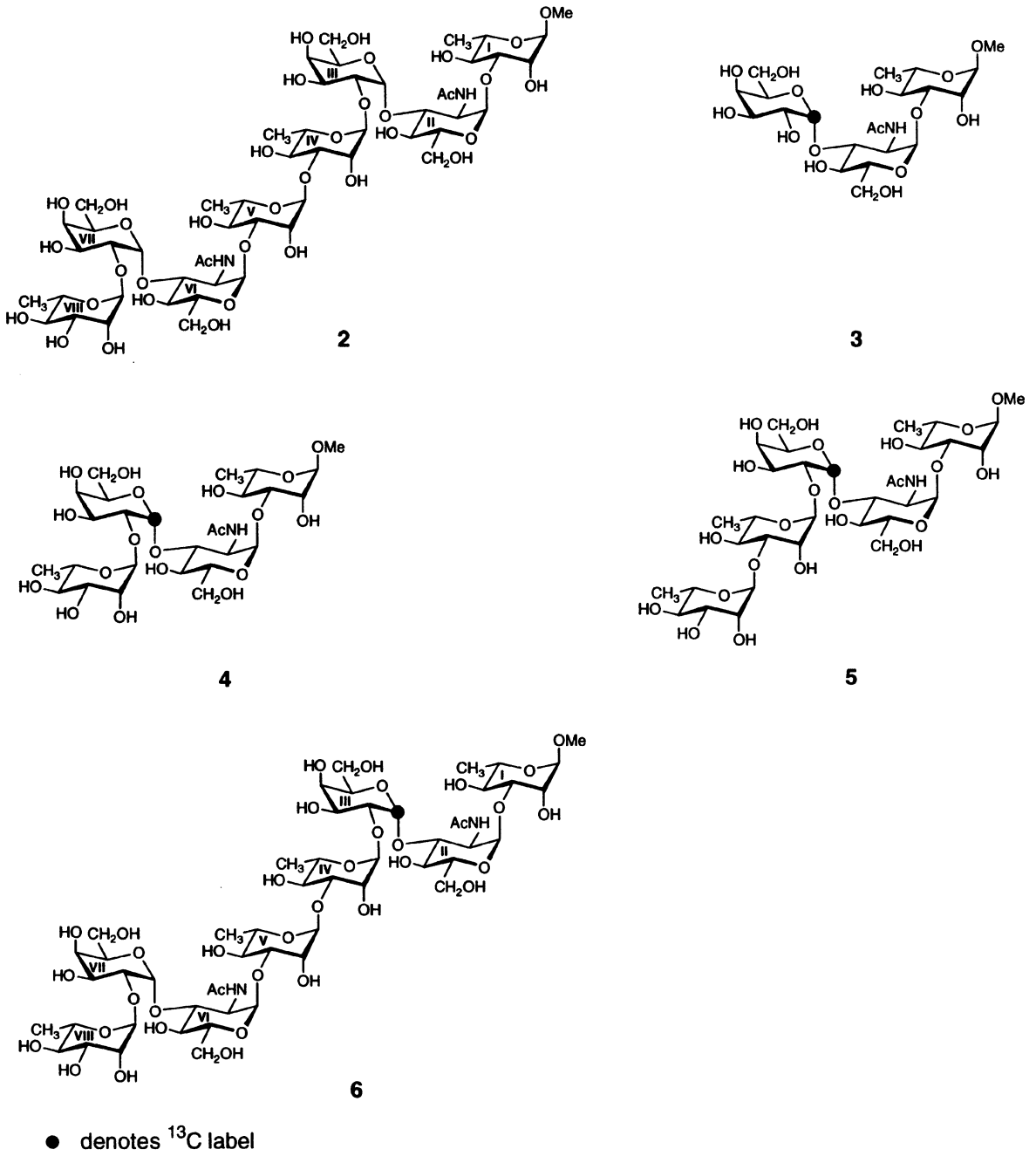

Scheme 1.

Table 1
^{1}H NMR chemical shifts [a] of the octasaccharide methyl glycoside **2**

Proton	Residue [b]							
	Rha^{VIII}	Gal^{VII}	GlcN^{VI}	Rha^{V}	Rha^{IV}	Gal^{III}	GlcN^{II}	Rha^{I}
H-1	5.077	5.596	5.041	5.105	5.053	5.596	4.991	4.715
H-2	4.065	3.953	4.130	4.229	4.166	3.941	4.136	4.081
H-3	3.792	3.865	4.084	3.936	3.872	3.882	4.068	3.789
H-4	3.474	4.005	3.786	3.547	3.553	4.008	3.786	3.519
H-5	3.854	3.913	4.022	3.890	3.890	3.913	4.004	3.712
H-6	1.298	3.747	3.814	1.337	1.300	3.747	3.807	1.323
H-6′		3.753	3.814			3.753	3.807	
CH_3O								3.394
CH_3CON			2.059				2.050	

[a] δ values ± 0.002 ppm estimated standard uncertainty for a solution in deuterium oxide measured at 600 MHz.
[b] Rha, α-D-rhamnopyranosyl; Gal, α-D-galactopyranosyl; GlcN, 2-acetamido-2-deoxy-α-D-glucopyranosyl.

studied the solution conformation of a disaccharide fragment [13] that was found to be the minimum structure necessary to display significant binding (K_a 5.8×10^3 L/mol) with a monoclonal antibody directed at the native polysaccharide [11]. One immediate goal of the current study was to use NMR spectroscopy to define distance and dihedral angle constraints that could be used in molecular modeling computations to determine a conformation for the octasaccharide glycoside **2**. A further goal was to obtain ^{13}C NMR assignments, and to measure ^{13}C spin–lattice relaxation times (T_1) for the sugar residues, thus allowing the calculation of an approximate molecular correlation time that could be used for interpretation of the nuclear Overhauser effects.

2. Results and discussion

NMR spectroscopy.—The octasaccharide methyl glycoside **2** has been studied at 400, 500, and 600 MHz by a variety of techniques. Complete ^{1}H NMR assignments were generated by application of selective 1D TOCSY [14], DIPSI [15], 2D COSY [16], TOCSY [14], and *J*-resolved [17] techniques, and ^{13}C assignments by 2D HETCOR [18], gradient enhanced 2D HSQC-TOCSY [19] and decoupled HMBC (D-HMBC) [20] methods. Inter-proton distances have been obtained from studies of gradient-enhanced and non-gradient 2D NOESY [21], ROESY [22], and T-ROESY [23] ^{1}H NMR spectra.

Because of the similarity of some of the H-1 chemical shifts (see Table 1), the 1D TOCSY experiments performed by selective excitation of the H-1 protons were not totally selective, and confirmation of the assignments was obtained by the 2D TOCSY and *J*-resolved methods. In the methyl cross-peak region of the 2D TOCSY spectrum (see Fig. 1), the signals of the similar rhamnose residues are differentiated particularly well. On the other hand, the selective 1D DIPSI technique was found to be particularly useful for extended transmission of magnetization in the GlcN residues, so that complete sub-spectra for these residues could be obtained by this technique. By this means, an intense doublet was observed for the equivalent H-6 and H-6′ protons (for example, see Fig. 2). Nevertheless, the 1D DIPSI method was not found to be useful for improving the transmission of magnetization via the small $J_{4,5}$ coupling constant (1.0 Hz) in the Gal^{III} and Gal^{VII} residues[1] [24], so that for these residues, selective irradiation of H-1 still gave H-6 and H-6′ signals that were weak to unobservable. The ^{1}H chemical shifts and coupling constants measured by analysis of the ^{1}H NMR spectra of **2** are shown in Tables 1 and 2, respectively. As observed previously for many other oligosac-

[1] The hexose residues are labeled I, II, III…VIII, starting at the methyl glycoside end of the octasaccharide molecule according to Rule 2-carb-37.2 in Nomenclature of Carbohydrates, 1996 Recommendations (see *Carbohydr. Res.* 297 (1997) 1–92; http://www.chem./gmw.ac.uk/iupac/2carb).

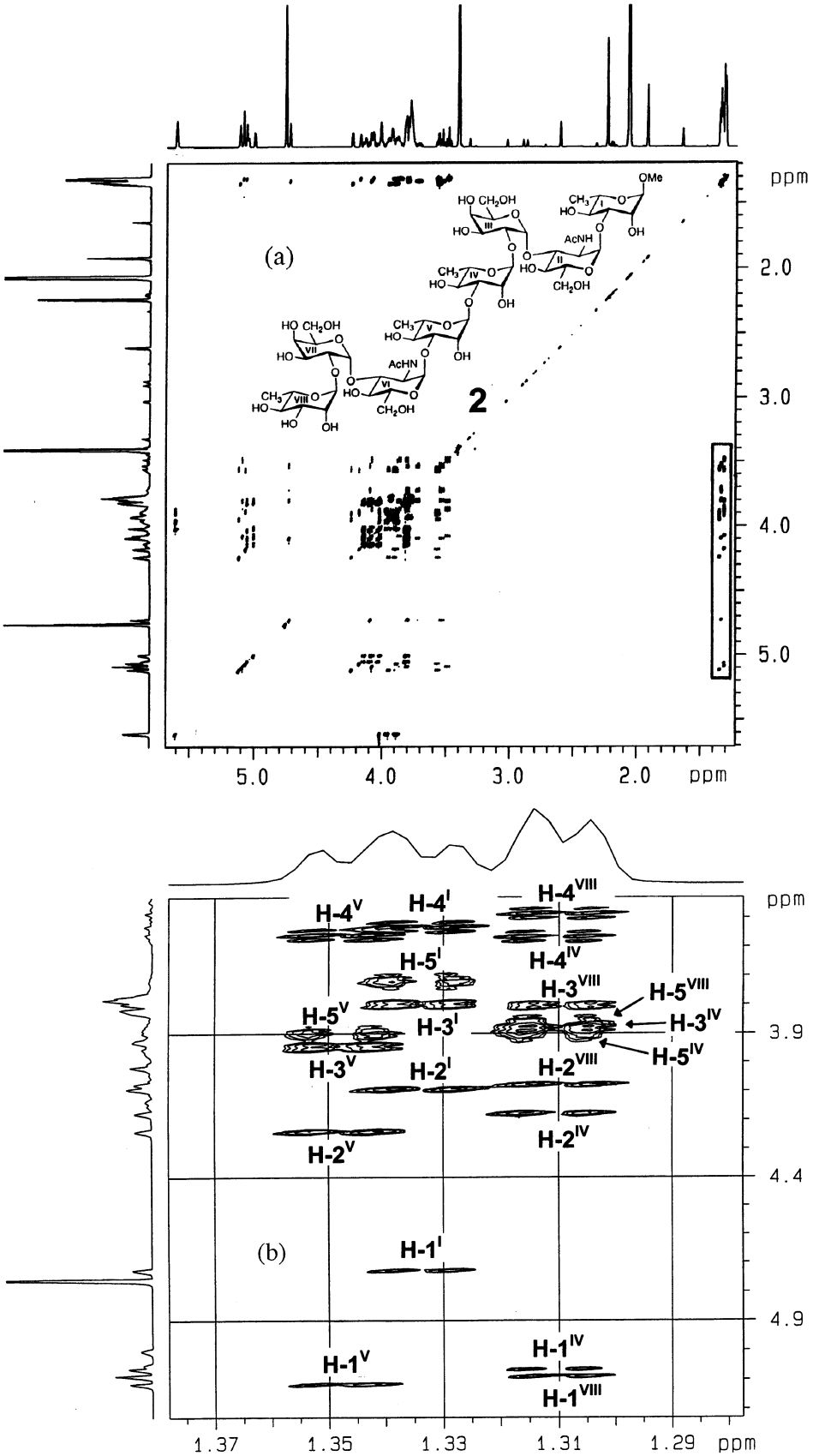

Fig. 1. 2D TOCSY ^{1}H NMR spectra of the octasaccharide methyl glycoside **2** at 600 MHz. (a) Complete contour plot and projections, and (b) an expansion of the boxed area in (a) showing dispersion of the signals of the protons with connectivity to the four rhamnose methyl groups and the detailed assignments for these protons.

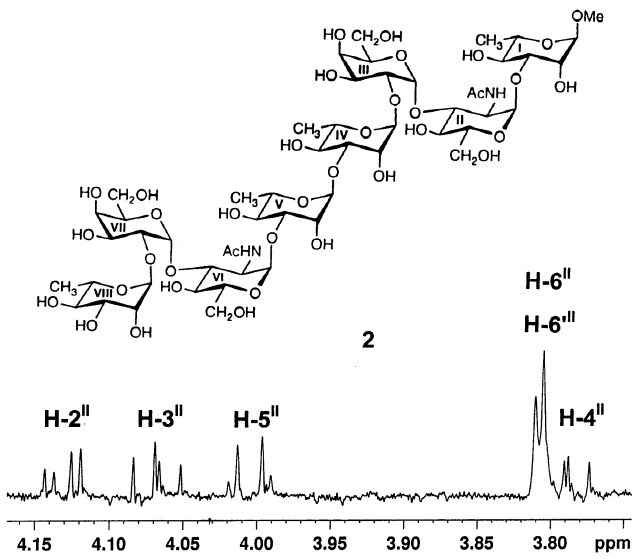

Fig. 2. Selective 1D DIPSI sub-spectrum for H-1^{II} of the GlcN^{II} residue of the octasaccharide methyl glycoside **2** at 600 MHz, showing facile transmission of magnetization to H-6^{II} and H-6′^{II}.

charide homologs in this series [6,7,9], the H-1 signal of the residue bearing the methyl glycoside resonates at substantially higher field than the other H-1 signals (see Table 1). However, at 600 MHz, the H-1 resonances in the chemically similar Gal^{III} and Gal^{VII} residues are coincident, as are the H-5, H-6, and H-6′ pairs of signals of these residues. A number of other accidental chemical shift equivalences were observed, including H-4^{II} and H-4^{VI}, H-5^{IV} and H-5^{V}, H-6^{II} and H-6′^{II}, and H-6^{VI} and H-6′^{VI} (see Table 1). The vicinal coupling constants for **2** (see Table 2) indicate that its hexose residues exist in the pyranose chair forms depicted in Scheme 1 [25].

In Table 3 are shown the ^{13}C chemical shift assignments for **2**, together with the spin–lattice relaxation times (T_1) measured for the hexose ^{13}C nuclei. Analysis of the ^{1}H coupled ^{13}C spectrum of **2** yielded the $^1J_{C\text{-}1,H\text{-}1}$ values 170.0, 172.0, 175.4, 172.5, 170.7, 172.0, 175.6, and 172.6 ± 0.3 Hz estimated standard uncertainty, for residues I, II, III, IV, V, VI, VII, and VIII, respectively. These values are consistent with the α configuration for all the anomeric linkages, including the methyl glycoside [26].

From the data in Table 3, it may be seen that the methine, methylene, and methyl ^{13}C nuclei of **2** display T_1 values in the ranges 212–305, 140–177, and 449-506 ms, respectively, ranges which appear to be characteristic of the number of attached hydrogen atoms. It may be surmised that the T_1 values of the methylene ^{13}C nuclei are shorter than those of the methine ^{13}Cs because of relaxation of the methylene ^{13}Cs by dipolar interaction with two directly attached protons [27]. On the other hand, dipolar relaxation of the methyl ^{13}C nuclei by the methyl protons is expected to be less effective because of free rotation of the methyl groups, so that the less effective spin-rotation relaxation mechanism is dominant [28]. The increased mobility expected for the terminal residues of the linear octasaccharide **2** appears to be reflected in the ^{13}C T_1 values for the C-1, C-2, and C-3 nuclei, but is less pronounced for the C-4 and C-5 nuclei. Thus, the terminal residues (I and VIII) of **2** show C-1, C-2, and C-3 T_1 values in the range 256–305 ms, whereas the internal residues (II–VII) display such values in the range 215–

Table 2
^{1}H–^{1}H NMR coupling constants [a] of the octasaccharide methyl glycoside **2**

$J_{H,H}$	Residue							
	Rha^{VIII}	Gal^{VII}	GlcN^{VI}	Rha^{V}	Rha^{IV}	Gal^{III}	GlcN^{II}	Rha^{I}
$J_{1,2}$	1.7	3.8	3.6	1.9	1.8	3.8	3.7	1.9
$J_{2,3}$	3.5	10.4	10.6	3.2	3.4	10.3	10.5	3.4
$J_{3,4}$	9.8	3.3	8.6	9.7	9.6	3.3	8.6	9.7
$J_{4,5}$	9.6	1.0	10.1	9.9	9.7	1.0	10.1	9.8
$J_{5,6}$	6.5	5.0	[b]	6.4	6.4	5.0	[b]	6.3
$J_{5,6'}$	6.5	6.5	[b]	6.4	6.4	6.5	[b]	6.3

[a] Values in Hz ± 0.1 Hz estimated standard uncertainty measured at 600 MHz.
[b] Not measurable because of equivalent H-6 and H-6′.

Table 3
^{13}C NMR chemical shifts [a] and spin–lattice relaxation times [b] of the octasaccharide methyl glycoside **2**

^{13}C nucleus	Residue							
	Rha^{VIII}	Gal^{VII}	$GlcN^{VI}$	Rha^{V}	Rha^{IV}	Gal^{III}	$GlcN^{II}$	Rha^{I}
C-1	102.28	98.38	94.83	102.70	102.16	98.38	94.83	101.43
	(282 ± 14)	(233 ± 8)	(229 ± 4)	(223 ± 16)	(218 ± 20)	(233 ± 8)	(229 ± 4)	(305 ± 25)
C-2	70.60	74.39	52.68	67.41	70.30	74.51	52.68	67.17
	(300 ± 14)	(228 ± 10)	(224 ± 8)	(233 ± 13)	(224 ± 20)	(215 ± 17)	(224 ± 8)	(283 ± 19)
C-3	70.82	69.73	75.15	75.60	78.81	69.73	75.49	75.70
	(256 ± 21)	(233 ± 5)	(227 ± 20)	(228 ± 10)	(221 ± 17)	(233 ± 5)	(237 ± 10)	(284 ± 14)
C-4	72.63	70.19	71.82	71.01	71.99	70.19	71.82	71.08
	(245 ± 5)	(243 ± 6)	(236 ± 7)	(290 ± 17)	(229 ± 11)	(243 ± 6)	(236 ± 7)	(212 ± 9)
C-5	69.95	71.60	72.66	69.73	70.06	71.60	72.61	69.21
	(243 ± 5)	(235 ± 7)	(245 ± 5)	(233 ± 5)	(226 ± 21)	(235 ± 7)	(245 ± 5)	(304 ± 14)
C-6	17.34	61.46	60.77 [c]	17.56	17.41	61.46	60.71 [c]	17.45 [d]
	(506 ± 20)	(177 ± 6)	(140 ± 20)	(472 ± 30)	(449 ± 21)	(177 ± 6)	(153 ± 27)	(472 ± 31)

[a] δ_C values ± 0.01 ppm estimated standard uncertainty for a solution in deuterium oxide measured at 100.6/400 MHz.
[b] Shown in parentheses as the mean of seven measurements in ms ± one standard uncertainty.
[c] Assignments interchangeable.
[d] The ^{13}C chemical shifts of the remaining substituents are $\boldsymbol{C}H_3O$, 55.57; $\boldsymbol{C}H_3CON$, 22.79; $CH_3\boldsymbol{C}ON$, 174.85, 174.90.

237 ms. For C-4 and C-5, the terminal residues show T_1 values of 212–304 ms, and the internal residues 229–290 ms. Also noteworthy is the observation that the longest $^{13}CH_3$ T_1 value is that of the terminal C-6^{VIII} (see Table 3).

From the data in Table 3, an average T_1 value of 227.5 ms was calculated for the ^{13}C-1 nuclei in the six internal residues II–VII. The insertion of this value into the equation [27]

$$\tau_c = 16\pi^2 r_{C-H}^6/\gamma_C^2\gamma_H^2\hbar^2\mu_0^2 T_1 \quad (1)$$

together with an average value $r_{C\text{-}1\text{–}H\text{-}1}$ 1.10 Å determined for residues II–VII by modeling of **2**, yielded a correlation time τ_c 2.16×10^{-10} s for the internal portion of the octasaccharide molecule. This value is of the same order as the correlation time τ_c 2.97×10^{-10} s calculated for the zero-crossing point of the NOE (η_{max}) versus $\omega\tau_c$ curve for[2] $\omega = 2\pi \times 600.13$ rad/s, by use of the equation [29] $\omega\tau_c = (5/4)^{1/2} \approx 1.12$. Comparison of the magnitudes of these correlation times suggests that **2** should show NOESY cross-peaks that are weak, but slightly positive, i.e., of opposite sign to the diagonal cross-peaks. However, we found experimentally that the NOESY cross-peaks were indeed weak, but had the same sign as the diagonal cross-peaks, thus indicating that the octasaccharide lies slightly towards the 'large molecule' side of the NOE versus $\omega\tau_c$ curve [29]. This discrepancy may be attributed to the likely presence of some anisotropic tumbling of the octasaccharide molecule in solution, because Eq. (1) is based on the assumption of a rigid molecule tumbling isotropically, i.e., with no favored axis of rotation. With a molecular weight of 1346 g/mol, the octasaccharide molecule lies in the mass range 1–2 kg/mol in which the NOE is known to change rapidly with $\omega\tau_c$ [30].

Previous studies of the ^1H and ^{13}C chemical shifts and ^{13}C–^1H coupling constants of a series of synthetic oligosaccharide fragments of the O-polysaccharide of *S. dysenteriae* type 1 have indicated the likelihood of a conformational change in the vicinity of the linkage between the Gal and GlcN residues on going from the trisaccharide to the higher homologs in this series [7,9]. Therefore, the generation of a dihedral angle constraint for this linkage was of special interest. In previous work [4], the $^3J_{CH}$ coupling constants across this linkage were measured by 2D *J*-resolved NMR spectroscopy of the tri- (**3**), tetra- (**4**), and pentasaccharide (**5**) analogs that were specifically ^{13}C labeled at C-1 of the Gal residue glycosidically linked to a GlcN residue (see Scheme 1). The measured values of $^3J_{C\text{-}1(III),H\text{-}3(II)}$ also

[2] For a Larmor frequency of 500.13 MHz, the corresponding value is $\tau_c = 3.56 \times 10^{-10}$ s.

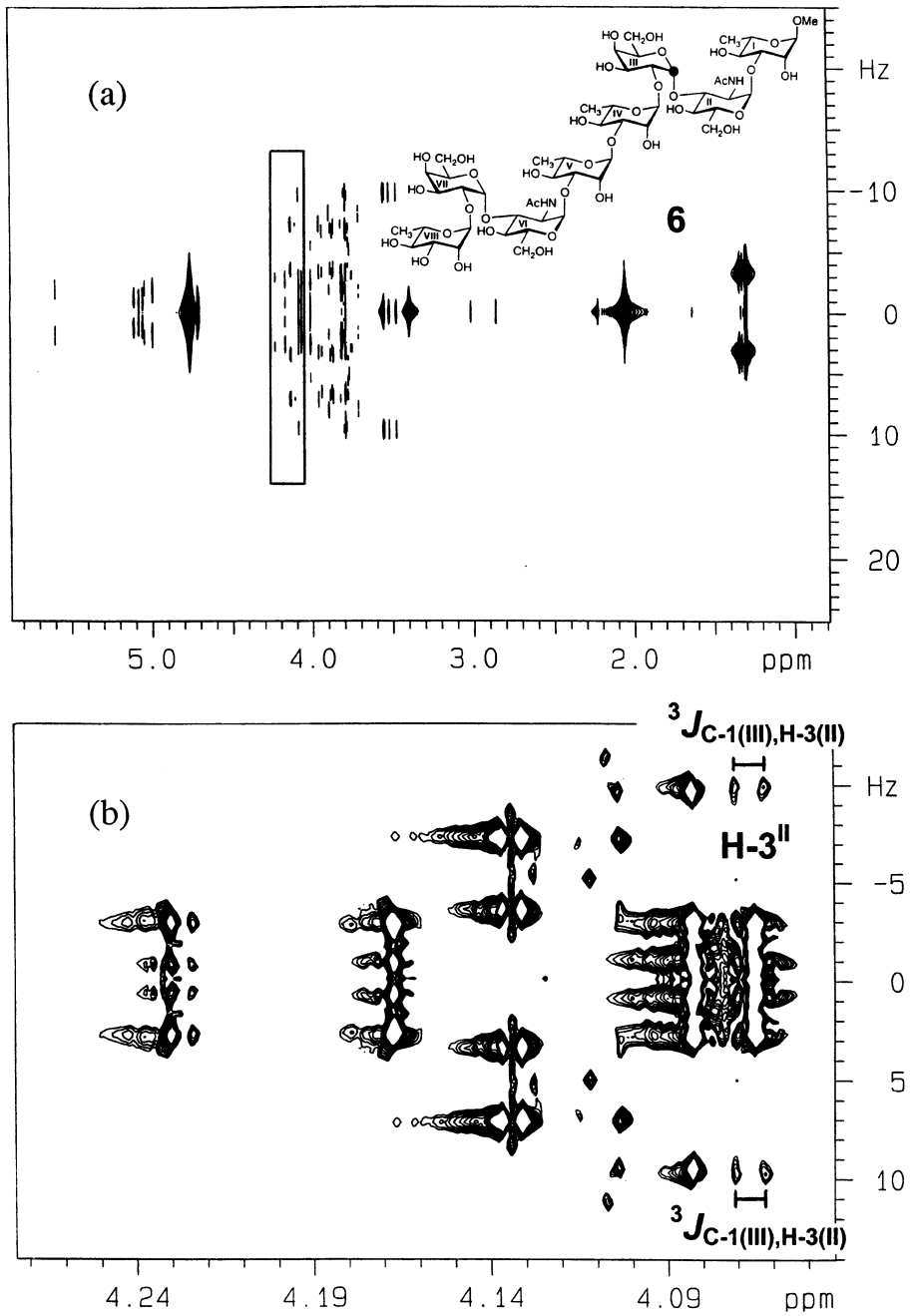

Fig. 3. 2D *J*-resolved ^{1}H NMR spectra of the ^{13}C labeled, octasaccharide methyl glycoside **6** at 500 MHz. (a) The full spectrum with the position of the ^{13}C label in the structure indicated by ●, and (b) expansion and amplification of the boxed region containing the H-3^{II} multiplet, showing resolution of the coupling constant $^3J_{C\text{-}1(III),H\text{-}3(II)}$ 4.0 ± 0.1 Hz.

reflected a conformational difference between the trisaccharide on the one hand, and the tetra- and pentasaccharide on the other, a difference that could be important in assessing how closely the conformations of the lower oligosaccharide homologs resemble that of the O-polysaccharide.

For similar measurements of the inter-glycosidic $^3J_{C\text{-}1(III),H\text{-}3(II)}$ coupling constant relating to the conformation of **2**, the octasaccharide methyl glycoside **6**, having a ^{13}C label (isotopic purity > 99 atom%) at C-1 of just one of its D-galactose residues (Gal^{III}, see Scheme 1), has been synthesized in an analogous manner to the parent octasaccharide **2** [8]. The spacing $^3J_{C\text{-}1(III),H\text{-}3(II)}$ 4.0 ± 0.1 Hz estimated standard uncertainty was readily detected in a pair of doublets in the F_2 dimension of the 2D *J*-re-

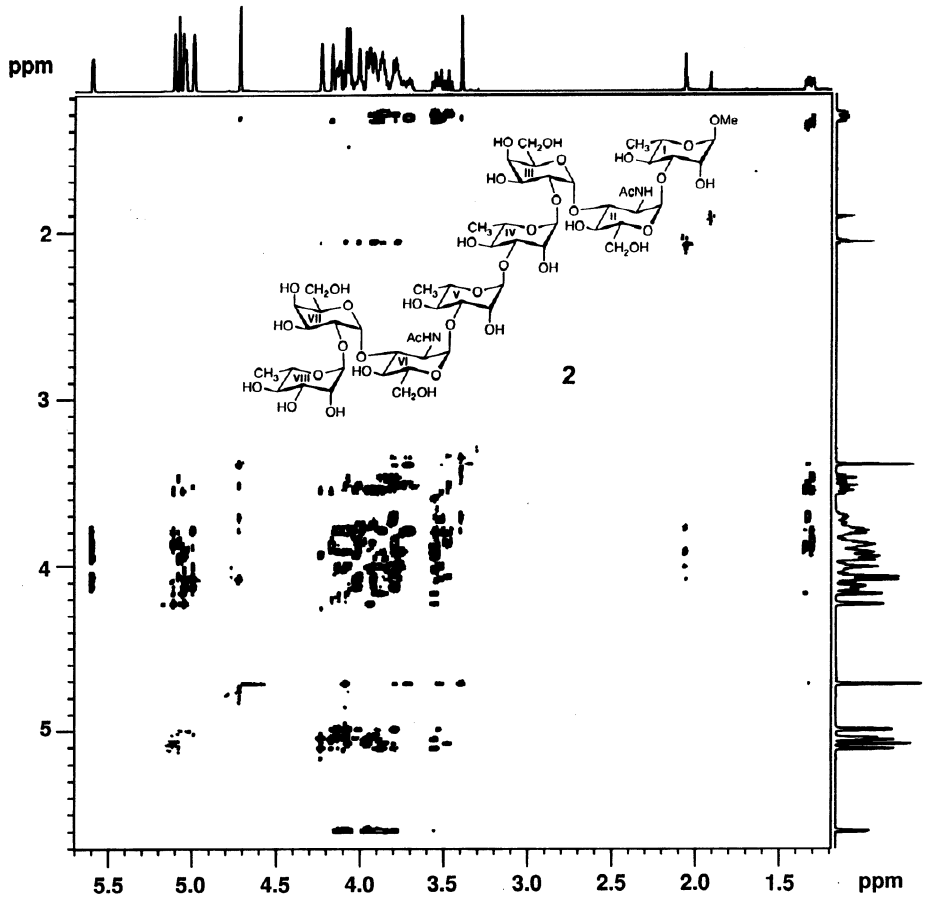

Fig. 4. 2D T-ROESY z-gradient enhanced ^{1}H NMR spectrum and projections of the octasaccharide methyl glycoside **2** at 600 MHz.

Table 4
Ring atom dihedral angle restraints (°) [a] used in restrained molecular dynamics of **2**

Dihedral angle defined by four ring atoms	Residue							
	VIII	VII	VI	V	IV	III	II	I
O-5,C-1,C-2,C-3	−57.1	53.2	57.5	−57.5	−52.7	57.7	59.0	−46.8
C-1,C-2,C-3,C-4	56.1	−52.7	−55.5	55.3	51.5	−55.8	−57.4	48.3
C-2,C-3,C-4,C-5	−54.8	54.2	53.7	−53.2	−51.9	53.9	54.7	−52.7
C-3,C-4,C-5,O-5	54.7	−57.7	−53.5	53.6	54.8	−54.9	−53.6	56.4
C-4,C-5,O-5,C-1	−59.5	61.3	58.8	−59.6	−60.2	59.8	58.0	−58.0
C-5,O-5,C-1,C-2	60.7	−58.2	−61.1	61.4	58.4	−60.6	−60.8	52.8

[a] Measured in the INSIGHT/DISCOVER software from an energy-minimized model of **2**.

solved ^{1}H NMR spectrum of **6** (see Fig. 3). Application of the Karplus equation [31], $^3J_{C,H} = 5.7\cos^2\psi - 0.6\cos\psi + 0.5$, gave the two possible values, $\psi_{C\text{-}1(III),H\text{-}3(II)}$ 33 and 137°. For reasons discussed previously [4], we favor the smaller of these two values, and this value (33°) was used as a dihedral angle restraint in the modeling calculations.

Information on internuclear distances in the octasaccharide was more usefully obtained from the 2D ROESY ^{1}H NMR spectra than from the 2D NOESY spectra, because of the low intensity of the NOESY cross-peaks mentioned previously. A comparison of conventional 2D ROESY ^{1}H NMR spectra measured with or without gradients, with 2D T-ROESY spectra measured with gradients (see Fig. 4) was found to be useful for identifying and/or diminishing low levels of anti-phase cross-peaks generated by the TOCSY mechanism,

particularly in the central region of the spectrum.

Molecular modeling.—Three types of structural constraints were used in an effort to define the conformation of **2** by molecular dynamics with simulated annealing. Rather than attempting to calculate proton–proton dihedral angles from vicinal $^1H-^1H$ coupling constants by use of a Karplus equation, a procedure that is heavily parameter dependent, we first modeled the octasaccharide structure with the chair forms indicated by the vicinal coupling constants (Table 2). The *ring atom* dihedral angles (see Table 4) were then computed from the energy-minimized model, and were used as dihedral angle constraints. The use of ring atom dihedral angle constraints was necessary in the molecular dynamics computations, because in their absence some of the hexopyranose rings tended to adopt skew boat or inverted chair forms that were clearly incorrect. Secondly, a set of inter-residue proton–proton distance restraints (see Table 5) was calculated from the intensities of the inter-residue proton cross-peaks in a 2D ROESY ^1H NMR spectrum of **2** (see Section 3). No attempt was made to use intra-residue ROEs to generate restraints. Thirdly, a single heteronuclear dihedral angle constraint $\psi_{C\text{-}1(III),H\text{-}3(II)}$ 33° was added to the restraints file.

Table 5
Inter-residue $^1H-^1H$ distances for **2**

Atom pair	Distance constraint (Å) from ROE intensity	Distance (Å) in the simulated structure
II-Ac/V-2 [a]	6.17	7.05
II-1/I-2	3.34	3.87
VI-1/V-2	3.52	3.04
VIII-1/VII-4	4.66	5.02
IV-1/III-4	5.00	5.36
V-1/IV-2	5.25	4.73
V-1/IV-4	3.45	3.81
VI-1/V-4	4.53	4.60
VIII-1/VII-2	2.92	2.84
IV-1/III-2	3.09	2.87
VIII-1/VII-3	2.97	3.60
V-1/IV-3	3.15	2.82
II-1/I-4	3.87	4.12
VII-1/VIII-4	3.98	4.90
III-1/IV-4	4.08	4.92
IV-2/V-3	4.40	4.15
IV-2/III-3	3.96	3.83
II-1/I-3	3.51	2.59
II-1/I-5	3.84	4.49
VI-1/V-3	3.88	3.17
IV-1/III-3	3.12	3.70
VI-1/V-5	4.07	5.39
II-Ac/I-2	5.90	5.70
VI-Ac/VII-3	5.14	5.49
II-Ac/III-2	5.83	6.16
VI-Ac/VII-2	5.22	5.14
VI-Ac/VII-5	4.41	4.31
VI-Ac/VII-6′	4.68	4.65
II-Ac/III-6′	5.05	5.44

[a] Labeling: II-Ac, N-acetyl proton of residue II; V-2, H-2 of residue V.

Restrained molecular dynamics with simulated annealing yielded the structure shown in Fig. 5, which is characterized by the $^1H-^1H$ distances reported in the right column of Table 5, and the inter-residue dihedral angles ϕ and ψ listed in Table 6. The variable extent to which the ROE-derived distance restraints are satisfied may be assessed by comparison of the distance restraints with the distances in the simulated structure in Table 5. The structure appears to be a short, irregular spiral, with all of the methyl substituents (HCMe, NAc, and OMe) on the exterior of the molecule. By starting with this structure, quenched molecular dynamics at 1000 K and energy minimization yielded a conformation of similar general shape, but with some of the residues rotated about the inter-glycosidic linkages, thus suggesting the possible presence of multiple minima or flexibility in these linkages. Inspection of the inter-residue dihedral angles reported in Table 6 reveals that the disaccharide repeating units of the octasaccharide do not necessarily show similar ϕ and ψ values. For example, the Gal^{VII},$GlcN^{VI}$ disaccharide subunit shows ϕ 61°, whereas the Gal^{III},$GlcN^{II}$ subunit has ψ −72°. Similarity of such values would only be expected if the orientation about the inter-glycosidic linkage is controlled solely by the short range, steric and electronic interactions about this linkage. However, longer-range attractive and repulsive interactions and hydrogen-bonding interactions between non-bonded residues obviously must be considered also, and these interactions may be expected to modify the energetics that result from particular linkage orientations.

Fluorescence studies of the binding of the series of oligosaccharides with a Fab antibody raised against *S. dysenteriae* type 1 have

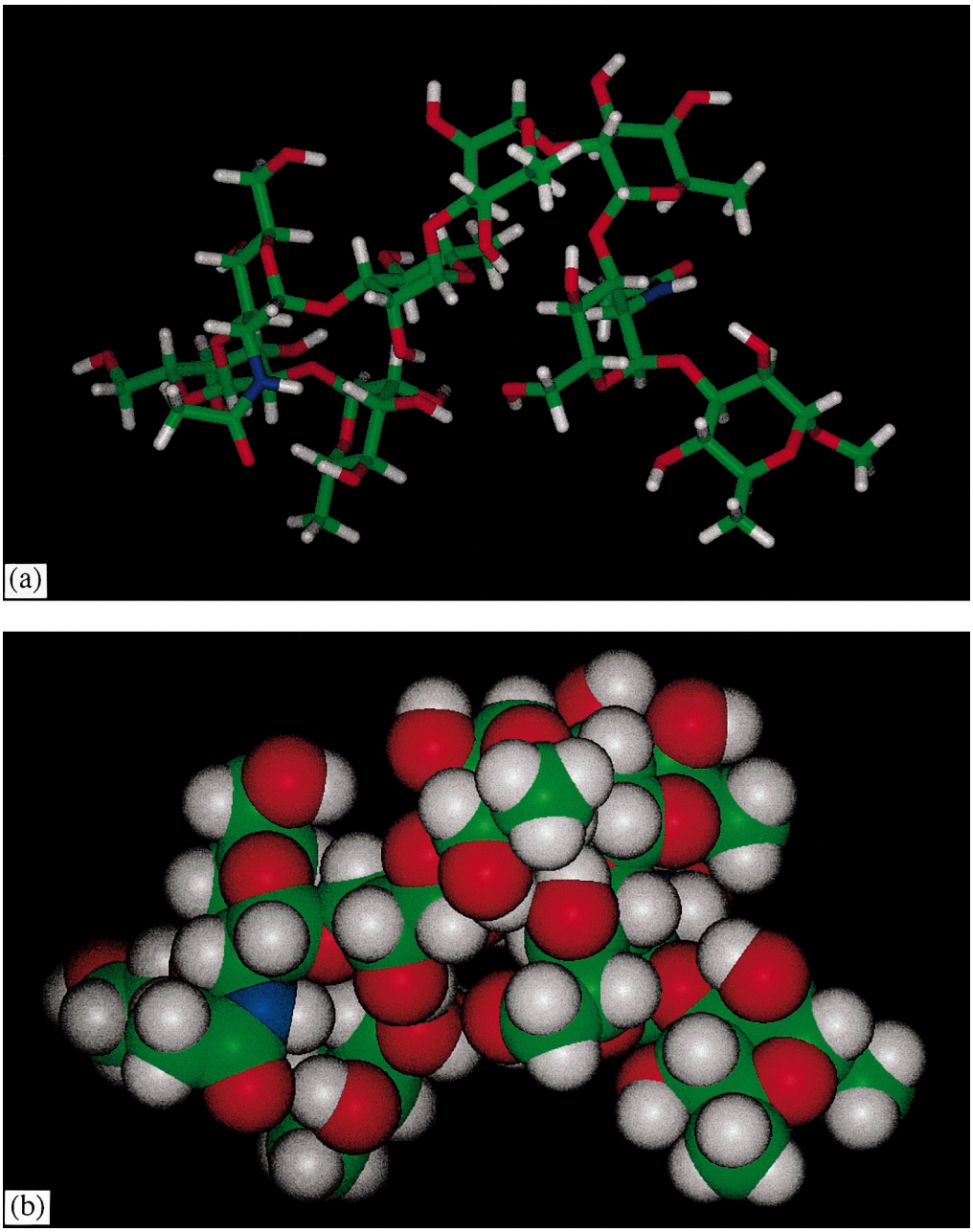

Fig. 5. The structure of the octasaccharide derivative **2** obtained by restrained molecular dynamics with simulated annealing, with the methyl glycoside oriented towards the lower right. (a) A stick model, and (b) a space-filling model.

Table 6
Inter-residue dihedral angles (°) [a] in the structure of **2** obtained by restrained molecular dynamics

Dihedral angle	Residue pair							
	VIII,VII	VII,VI	VI,V	V,IV	IV,III	III,II	II,I	I,OMe
ϕ, H-1,C-1,O-1,C-X	78	61	−74	72	68	−72	−35	42
ψ, C-1,O-1,C–X,H–X	19	30	−31	20	5	25	42	

[a] Measured in the INSIGHT/DISCOVER program.

shown that the Rha and Gal residues are important components of the antigenic determinant [11]. Taken with the exterior location of the rhamnose methyl groups, this suggests that binding of the oligosaccharides with the antibody may include hydrophobic interactions involving the methyl groups. It is recognized that the conformation determined for an oligosaccharide by restrained molecular dynamics may be 'virtual', because the effects of flexibility and possible conformational equilibria are undefined [32,33]. However, as has been emphasized previously [33], a restrained conformation may be a useful starting point from which to visualize the dynamic behavior of an oligosaccharide.

3. Experimental

Synthesis.—General experimental conditions are described in Refs. [2] and [4].

NMR spectroscopy.—Five-mm sample tubes were used. NMR spectroscopy of compound **2** was performed at a solution concentration of 27 mg in 0.5 mL of deuterium oxide, whereas **6** was examined at a concentration of 16 mg in 0.5 mL of deuterium oxide. ^{1}H and ^{13}C chemical shifts were referred to tetramethylsilane (TMS) by the addition of acetone to the solutions as a secondary, internal reference that was set to δ_H 2.225, and δ_C 31.0. ^{1}H NMR spectra were measured at 400, 500, and 600 MHz and at 300 K by the use of Bruker Instruments[3] NMR spectrometer models WM-400, AMX-500, AMX-600, DRX-500, or DRX-600. The data were acquired and processed by means of the Bruker DISR (WM-400), UXNMR (AMX-500 and AMX-600) or XWINNMR (DRX500 and DRX-600) programs running on either the Bruker Aspect 3000 or X32 computers, or the Silicon Graphics Inc. computer models Indy R4600 or O2 R5000.

1D ^{13}C NMR spectra were recorded at 100.6/400 MHz and at 301 K by use of the Bruker WM-400 spectrometer, with continuous, WALTZ-16 [34] composite pulse ^{1}H decoupling (CPD), unless otherwise stated. A spectral width of 20 kHz was used, together with a 32768 point data set, and a $\pi/6$ pulse (3.2 μs). A proton-coupled ^{13}C NMR spectrum was obtained with NOE, by use of gated CPD with a $\pi/2$ pulse (9.6 μs). Selective 1D ^{1}H TOCSY, and 2D heteronuclear $^{13}C-^{1}H$ correlation, 2D $^{1}H-^{1}H$ COSY, NOESY, ROESY, TOCSY, and *J*-resolved NMR experiments were performed as described previously [9], except that for selective 1D TOCSY, the Gaussian selective pulse width was 400 ms, and the isotropic mixing time was 200 ms. For 2D ROESY spectra, the B_1 radio-frequency field strength for spin-locking was 1800 Hz. Selective 1D ^{1}H DIPSI spectra were acquired at 600 MHz by using the DIPSI-2 isotropic mixing sequence [15] with a 400 ms mixing time, a low-power Gaussian selective pulse width of 420 ms defined by 1024 points, phase-gradient-induced frequency offsets for selective excitation of anomeric protons, a spectral width of 3.1 kHz, a 16,384 point data set, and 160 scans preceded by four dummy scans.

2D T-ROESY NMR spectra were acquired by use of a *z*-gradient pulse sequence, together with 2048 (F_2) × 1024 (F_1) data sets zero-filled to 2048 points in the F_1 dimension, a spectral width of 3.1 kHz in both dimensions, a mixing time of 1 s, and 40 scans preceded by 160 dummy scans. The data were processed in the echo/anti-echo mode, with sine-bell windows shifted by $\pi/2$ rad applied in both dimensions.

Gradient-enhanced 2D HSQC-TOCSY experiments were performed at 500 MHz and 303 K, by using 1024 (F_2) × 256 (F_1) point data sets, spectral widths of 5.48 and 100 ppm in the ^{1}H and ^{13}C dimensions, respectively, with ^{1}H and ^{13}C $\pi/2$ pulse widths of 10.7 and 15.5 μs, respectively, 32 scans per FID, and a recycle delay of 1.5 s. A DIPSI-2 mixing sequence was used with a mixing time of 98 ms, and GARP ^{13}C decoupling during acquisition. Echo/anti-echo coherence selection was used in the F_1 dimension, and the strongest field gradient pulse used was sine-bell shaped, at an amplitude of 40 G/cm, and a duration of 1 ms. Phase-sensitive processing was used, with

[3] Certain commercial equipment, instruments, or materials are identified in this paper to specify adequately the experimental procedure. Such identification does not imply recommendation by the National Institute of Standards and Technology, nor does it imply that the materials are necessarily the best for the purpose.

cosine-bell window functions applied in both dimensions.

Gradient-enhanced D-HMBC was carried out under the same conditions, except that a low-pass filter was used to suppress one-bond connectivities, 16 scans were acquired for each FID, a delay of 40 ms was allowed for development of multiple quantum coherences, and decoupling was employed during acquisition.

Measurement of ^{13}C spin–lattice relaxation times.—The ^{13}C spin–lattice relaxation times of **2** were measured at 100.6 MHz in the presence of continuous CPD at 400 MHz. The inversion recovery method [35] was used, with four cycles of 14 delay times equal to 0.l, 0.15, 0.2, 0.25, 0.3, 0.35, 0.4, 0.45, 0.5, 1.0, 1.5, 2.0, 2.5, and 3.0 s. A total of 1600 scans was used for each delay time, together with a spectral width of 20 kHz, a 16384 point data set, and a ^{13}C $\pi/2$ pulse width of 8.6 μs. The relaxation data were analyzed by means of the three-parameter, non-linear least-squares fitting routine in the Bruker DISR94 program, running on the Aspect 3000 computer.

Molecular modeling methods.—With the assumption of the 'isolated spin pair approximation' for each pair of protons a and b, the cross-peak intensities (I_{ab}) from 2D ROESY spectra measured at 500 MHz with a spin-lock field of 1800 Hz were generated in the Bruker AURELIA program [36] and were used to calculate inter-residue proton–proton distances (r_{ab}) for use as restraints. The reference distance (r_{rd} 3.89 Å) of H-2 and H-4 of Rha^{IV} in an energy-minimized model of **2** was chosen for the calculation of the r_{ab} distances because of the good resolution of the ROESY cross-peaks due to these protons. This approach uses the relationship [37] $I_{ab}/I_{rd} = (r_{ab}/r_{rd})^{-6}$, where I_{rd} is the intensity of the reference ROESY cross-peak. In terms of the accuracy of the derived distances, a larger reference distance is known to be better than a smaller one [38].

Energy calculations were performed by use of the Biosym/MSI INSIGHT II/DISCOVER software package, version 95.0, running on a Silicon Graphics Inc. Indigo 2 R4400 200 MHz computer. The computations were performed with implicit solvent by using the AMBER forcefield with Homans extensions for the anomeric atoms [39], with a distance-dependent, effective dielectric constant of 4.0. Initially, a steepest-descent energy minimization was conducted for 1000 steps. Interleaved restrained molecular dynamics (1000 equilibration steps of 1 fs, 5000 dynamics steps of 1 fs) and VA09A energy minimizations (1000 steps max) were then performed with simulated annealing. The following restraints were used: (a) 29 distance constraints; (b) 48 ring-atom dihedral angle restraints derived from the energy-minimized ring forms indicated by the vicinal $^1H-^1H$ coupling constants in Table 2, and (c) one inter-glycosidic dihedral angle restraint, $\psi_{C\text{-}1(III),H\text{-}3(II)} = 33°$. Simulated annealing was performed by heating the system initially to 1000 K, followed by 50 K decrements of the temperature down to 300 K, with restrained molecular dynamics and energy minimization at each temperature.

Methyl O-α-L-*rhamnopyranosyl-(1→2)*-O-α-D-*galactopyranosyl-(1→3)*-O-*(2-acetamido-2-deoxy-*α-D-*glucopyranosyl)-(1→3)*-O-α-L-*rhamnopyranosyl-(1→3)*-O-α-L-*rhamnopyranosyl-(1→2)*-O-α-D-*[1-^{13}C]-galactopyranosyl-(1→3)*-O-*(2-acetamido-2-deoxy-*α-D-*glucopyranosyl)-(1→3)*-α-L-*rhamnopyranoside* (**6**).—Compound **6** was synthesized essentially as reported for the unlabeled analog **2** [8] by condensation of two tetrasaccharide building blocks [2,4], except that the tetrasaccharide acceptor [4] contained a ^{13}C label at the anomeric position of the Gal residue. Compound **6** so obtained matched the physical ($[\alpha]_D$) and spectral (NMR and FABMS) properties of the parent compound **2**, except for the differences arising from the ^{13}C label.

Acknowledgements

Thanks are due Dr Wolfgang Bermel of Bruker Analytische Messtechnik for pulse sequences for 2D T-ROESY with gradients.

References

[1] V. Pozsgay, C. Chu, L. Pannell, J. Wolfe, J.B. Robbins, R. Schneerson, *Proc. Natl. Acad. Sci. USA*, 96 (1999) 5194–5197.
[2] V. Pozsgay, *J. Org. Chem.*, 63 (1998) 5983–5999.

[3] V. Pozsgay, *Angew. Chem.*, 110 (1998) 145–149; *Angew. Chem., Int. Ed. Engl.*, 37 (1998) 138–142.
[4] V. Pozsgay, N. Sari, B. Coxon, *Carbohydr. Res.*, 308 (1998) 229–238.
[5] V. Pozsgay, *J. Am. Chem. Soc.*, 117 (1995) 6673–6681.
[6] V. Pozsgay, B. Coxon, *Carbohydr. Res.*, 277 (1995) 171–178.
[7] V. Pozsgay, B. Coxon, *Carbohydr. Res.*, 257 (1994) 189–215.
[8] V. Pozsgay, L. Pannell, *Carbohydr. Res.*, 258 (1994) 105–122.
[9] V. Pozsgay, B. Coxon, H. Yeh, *Bioorg. Med. Chem.*, 1 (1993) 237–257.
[10] V. Pozsgay, C.P.J. Glaudemans, J.B. Robbins, R. Schneerson, *Bioorg. Med. Chem. Lett.*, 2 (1992) 255–260.
[11] V. Pavliak, E.M. Nashed, V. Pozsgay, P. Kovac, A. Karpas, C. Chu, R. Schneerson, J.B. Robbins, C.P.J. Glaudemans, *J. Biol. Chem.*, 268 (1993) 25797.
[12] C.E. Miller, A. Karpas, R. Schneerson, K. Huppi, P. Kovac, V. Pozsgay, C.P.J. Glaudemans, *Mol. Immunol.*, 33 (1996) 1217–1222.
[13] B. Coxon, N. Sari, L.A. Mulard, P. Kovac, V. Pozsgay, C.P.J. Glaudemans, *J. Carbohydr. Chem.*, 16 (1997) 927–946.
[14] A. Bax, D.G. Davis, *J. Magn. Reson.*, 65 (1985) 355–360.
[15] S.P. Rucker, A.J. Shaka, *Mol. Phys.*, 68 (1989) 509–517.
[16] W.P. Aue, E. Bartholdi, R.R. Ernst, *J. Chem. Phys.*, 64 (1976) 2229–2246.
[17] W.P. Aue, J. Karhan, R.R. Ernst, *J. Chem. Phys.*, 64 (1976) 4226–4227.
[18] A. Bax, *J. Magn. Reson.*, 53 (1983) 517–520.
[19] K.E. Kövér, V.J. Hruby, D. Uhrin, *J. Magn. Reson.*, 129 (1997) 125–129.
[20] K. Furihata, H. Seto, *Tetrahedron Lett.*, 36 (1995) 2817–2820.
[21] J. Jeener, B.H. Meier, P. Bachmann, R.R. Ernst, *J. Chem. Phys.*, 71 (1979) 4546–4553.
[22] (a) A.A. Bothner-By, R.L. Stephens, J.M. Lee, C.D. Warren, R.W. Jeanloz, *J. Am. Chem. Soc.*, 106 (1984) 811–813. (b) A. Bax, D.G. Davis, *J. Magn. Reson.*, 63 (1985) 207–213.
[23] T.-L. Hwang, A.J. Shaka, *J. Am. Chem. Soc.*, 114 (1992) 3157–3159.
[24] B. Coxon, H.G. Fletcher Jr., *Chem. Ind.*, (1964) 662–663.
[25] B. Coxon, *Tetrahedron*, 21 (1965) 3481–3503.
[26] K. Bock, C. Pedersen, *Acta Chem. Scand., Ser. B*, 29 (1975) 258–264.
[27] D. Neuhaus, M.P. Williamson, *The Nuclear Overhauser Effect in Structural and Conformational Analysis*, VCH, New York, 1989, p. 32.
[28] J.H. Noggle, R.E. Schirmer, *The Nuclear Overhauser Effect. Chemical Applications*, Academic Press, New York, 1971, p. 36.
[29] Ref. 27, p. 37.
[30] Ref. 27, p. 36.
[31] (a) B. Mulloy, T.A. Frenkiel, D.B. Davies, *Carbohydr. Res.*, 184 (1988) 39–46. (b) I. Tvaroska, M. Hricovini, E. Petrakova, *Carbohydr. Res.*, 189 (1989) 359–362.
[32] J.P. Carver, *Curr. Opin. Struct. Biol.*, 1 (1991) 716–720.
[33] S.W. Homans, in M. Fukuda, O. Hindsgaul (Eds.), *Molecular Glycobiology*, Oxford University Press, New York, 1994, p. 230.
[34] A.J. Shaka, J. Keeler, R. Freeman, *J. Magn. Reson.*, 53 (1983) 313–340.
[35] R.L. Vold, J.S. Waugh, M.P. Klein, D.E. Phelps, *J. Chem. Phys.*, 48 (1968) 3831–3832.
[36] K.-P. Neidig, M. Geyer, A. Görler, C. Antz, R. Saffrich, W. Beneicke, H.R. Kalbitzer, *J. Biol. NMR*, 6 (1995) 255–270.
[37] Ref. 27, p. 107.
[38] Ref. 27, p. 109.
[39] S.W. Homans, *Biochemistry*, 29 (1990) 9110–9118.